SAM Assisted Nickel-Boron Electroless Metallization of PDMS

A. Molazemhosseini, S. Ieffa, P. Vena, and L. Magagnin

Department of Chemistry, Chemical and Materials Engineering G. Natta, Politecnico di Milano, Via Mancinelli 7, Milan, Italy

Introduction

A growing range of applications has a critical need for electronic systems, which cannot be made through rigid wafer-based technology. These applications include flexible displays (1), flexible transistors/batteries/capacitors (2-4) and wearable health-monitoring biosensors (5-7). As intrinsically flexible materials have poor electrical performance, the dominant fabrication strategy is to exploit the flexibility of a polymer along with the electrical conductivity of a metal coating.

The widely used flexible substrates are poly (ethylene terephthalate) (PET), poly (ethylene naphthalate) (PEN), polyimide (PI), polycarbonate (PC) and polydimethylsiloxane (PDMS) (8-11). Metal deposition methods based on PVD, CVD or sputtering techniques are not desirable considering the complexity and process expenses. More importantly, regarding the possibility for roll-to-roll manufacturing and mass production, there is a growing demand in electronic industry toward all-wet metallization processes. Among these are mainly ink-jet printing and electroless deposition used for polymer substrates. Electroless deposition is a process for chemical deposition of metals from a solution containing a reducing agent, a desired metal ion and a complexing agent. The process is generally inexpensive and can be performed near room temperature in aqueous environment. The significant advantage of electroless deposition over ink-jet printing is the ability to deposit on substrates with complex shapes. Metals used in

electronics applications that can be deposited through electroless deposition include noble metals (e.g., Au, Ag, Pt, and Pd) and specific transition metals such as Cu and Ni (12).

To start the metal deposition, every insulator substrate must be catalyzed. Moreover, substrate surface treatment must be carried out in order to make the possibility for the surface to be catalyzed. There are various surface-oxidizing techniques for polymer substrates including UV/ozone treatments (10, 13), plasma oxidizing (14), solution treatments (8) or combination of those (9). Pd/Sn colloidal catalyst solution is the mostly used one to catalyze the oxidized polymer surfaces. The colloids consist of a palladium-rich core, which is the actual catalyst that initiates electroless metallization. A hydrolyzed Sn^{2+} /Sn^{4+} shell protect the core from oxidation. The chloride ions associated with this shell give the colloids a net negative charge to inhibit aggregation, and allow the colloids to be electrostatically bound to cationic functional groups on a substrate (15). Another approach to catalyze the surface is the two-step $SnCl_2$ sensitization and $PdCl_2$ activation (9). The Pd nuclei formed in these two approaches has poor adhesion to the substrate because of the absence of any chemical bond between the Pd catalyst and the substrate (16). Regarding environmental and economic considerations, it is desirable to have Sn-free one-step activation process however; it is not possible to directly chemisorb Pd on the surface. Ink-jet printing technique is also used to catalyze the insulator surfaces by transferring a conductive thin layer to the surface in order to act as a seed layer for further electroless metallization. This conductive layer can be silver ink (17), palladium ink (18), or may contain a salt of the metal which is desired to coat (19). However, inkjet-printing is not practical for the substrates with non-planar and complex shapes.

More recently, there has been a tendency to exploit the ability of self-assembled monolayers (SAM) in making covalent bonds with oxidized polymer substrates. SAMs are highly ordered two-dimensional structures that are formed spontaneously on a variety of surfaces. The most common SAM/substrate combinations are alkylsilanes on oxidized surfaces (20). SAMs can anchor to oxidized polymers through their hydrolysable groups at one end and adsorb metallic nanoparticles such as Pd on their functional groups at the other end. SAMs with $–NH_2$ and –SH functional groups have been used for plastic metallization (21, 22). Recently, Guo et al. used 3-aminopropyltrimethoxysilane (APTMS) for electroless Ni plating on polyester fabric. Formation of Pd-activated APTMS was demonstrated by X-ray photoelectron spectroscopy, and further Ni electroless deposition on activated polyester was showed to be successful (16). In another study, ultrasonic-assisted electroless copper metallization of PET has been carried out using 3-mercaptopropyltriethoxysilane (MPTMS). The affinity of -SH groups to Cu was exploited without any further need to use $PdCl_2$ activation step (9).

Among different plastic substrates to metallize, PDMS is one of the challenging ones due to its intrinsic low surface energy (19.8 mN/m at 20°C). Metallization of PDMS is usually carried out by evaporation processes such as e-beam and cluster beam deposition (23, 24). There are quite a few studies on wet metallization of PDMS. In the most significant one, a copper electroless metallization was carried out on a Pd-activated silanized PDMS (15). To our knowledge, this work is the first attempt to metallize PDMS with NiPB through a SAM assisted wet metallization process.

Experimental

Fabrication

All-wet metallization of polydimethylsiloxane (PDMS) (Sylgard 184 Dow Corning 10:1 ratio) was carried out through Nickel-phosphorous-Boron (NiPB) electroless deposition process. The electroless bath was a commercial Ni solution provided by Tecnochimica Italy (Table I). All the chemicals were produced by Sigma-Aldrich and used as received. PDMS surface modification was done by immersion of the samples in sodium hydroxide solution (1M) for at least 24 h followed by 10 min corona treatment (portable corona generator BD-20AV). The modified surface was then silanized by Self-assembled monolayers (SAM) of n-(2-aminoethyl) 3-aminopropyl-trimethoxysilane (AEAPTMS) in a 0.02% v/v toluene based solution. Silanized samples were then sonicated for 2 min in toluene and 12 min in DI water. Surface activation was performed by a 0.5 g/l solution of palladium chloride containing 10ml/l HCl. Sample with three lines of NiPB on PDMS (each line with 5mm width and 20mm length) was fabricated to act as an electrochemical ethanol sensor.

Characterization

Morphological inspections were carried out using scanning electron microscope (Zeiss EVO 50 and Stereoscan360 Cambridge Analytics). Surface topographic characterization was performed using an NT-MDT Solver Pro Atomic Force Microscope (AFM) instrument operated in non-contact mode. Glow discharge optical emission spectroscopy (SPECTRUMA GDA 750 analyzer) was used to characterize the metallized samples. Cyclic voltammetry and chronoamperometry studies for ethanol sensor characterization were carried out using an EG&G Princeton applied research potentiostat.

Results and Discussion

NiPB coating characterization

Fig. 1 shows the GDOES characterization results for NiPB coated PDMS. Silicon, carbon and oxygen signals after the depth of 80nm are attributed to PDMS substrate. Nickel and phosphorous signals in the first 80nm belong to NiPB coating. It is assumed that the amount of Boron in the coating is not high enough to be detectable by the instrument. As presented in Fig. 1b, three peaks were detected in lower intensities at the depth range of 50 to 80nm. The palladium peak confirms the presence of activation layer beneath the NiPB coating. Carbon and oxygen peaks are attributed to the SAM layer formed on PDMS substrate. The inability to detect any signal for nitrogen at the NiPB/PDMS interface may be attributed to smaller number of N atoms presented in SAM structure compared to C and O. The GDOES results confirm the formation of Pd-SAM activated interface.

Fig. 2 demonstrates AFM characterizations of PDMS after surface modification (Fig. 2a), silanization (Fig. 2b) and metallization (Fig. 2d). Fig. 2b presents SAM formation on PDMS. A multilayer SAM is achieved according to the average surface roughness. By comparing average surface roughness of Fig. 2b and c, it is concluded that, sonications in toluene and DI water were effective to remove the hydrogen bonded SAM molecules resulting in a more uniform layer with lower thickness close to a monolayer considering the theoretical length of AEAPTMS (≈ 0.8 nm (25)). Surface topography of the final NiPB coating is presented in Fig. 2d. A compact film with acceptable uniformity was achieved.

Fig. 3 shows cross sectional SEM observation of the coating. The breakage in the coating is due to the sample preparation process. (breakage after immersion in liquid nitrogen). According to Fig. 3a, none of the NiPB film islands was detached from the plastic substrate claiming an acceptable adhesion. In addition, evidences of irregular growth with nodular structures formation are visible in Fig. 3b which is in agreement with AFM characterizations (Fig. 2d).

Electrochemical characterization

Sample with three lines of NiPB on PDMS (each line with 5mm width and 20mm length) was fabricated to apply as an electrochemical ethanol sensor (Fig. 4). Each one the lines act as counter, reference and working electrodes. The surface area of the working electrode was $6\times6mm^2$. Potassium hydroxide solution (0.1M) was used as base media for electrochemical studies.

Fig. 5, shows cyclic voltammetry results for the ethanol sensor. The redox pair of $NiOOH/Ni(OH)_2$ were successfully formed on the working electrode. The oxidation peak of ethanol was achieved around 0.9V for 500ppm ethanol and tends to shift to higher voltages in higher ethanol concentrations. 1 V is selected as the fixed potential for later chronoamperometry characterizations.

Fig. 6 presents chronoamperometry results for the ethanol sensor carried out at room temperature under 200 rpm stirring. After stabilization of the current, ethanol was added every 100s. Each step corresponds to 100ppm increase in the ethanol concentration. The sensor response time was calculated as 20s which was the time needed to achieve the current equal to 90% of the maximum current after each addition. The lower detection limit for the sensor is achieved as 20ppm of ethanol. Fig. 7 shows the calibration curve for the sensor. The calibration curve was achieved using the currents measured after 50s of each ethanol addition. Each current was calculated as an average between three different measurements. A linear range up to 600ppm ethanol with $R^2=0.9972$ was obtained. The sensor sensitivity in the linear range is calculated as $6.9\mu A.ppm^{-1}.cm^{-2}$.

In order to examine the reproducibility of the results, 20 different sensitivity measurements were carried out for 20 times addition of 300ppm ethanol. As presented in Fig. 8, the variations in sensitivity is less than 10% which signifies an acceptable reproducibility of the results.

The interference studies were done in presence of citric acid, acetic acid and ascorbic acid as presented in Fig. 9. These acids may present in the system as the ethanol sensor needs to be used for medical or brewing applications. The highest interference is attributed to ascorbic acid. According to Fig. 9, sensor sensitivity to ethanol is about 7 times more than the highest interference measured. The results conclude the high selectivity of the sensor toward ethanol.

Conclusion

Wet metallization of PDMS was carried out through NiPB electroless deposition. A tin-free activation process using self-assembled monolayers was successfully employed on PDMS. A compact and uniform layer with acceptable adhesion was achieved after metallization. Through this process, the need for expensive evaporation processes was eliminated. A flexible electrochemical ethanol sensor with high sensitivity and selectivity

was fabricated based on NiPB/PDMS electrodes. Using the same Nickel coating as counter and reference electrodes contributes to fabrication of a simple cost-effective sensor.

References

1. G. P. Crawford, *John Wiley & Sons*, Ltd p. 51 (2005).
2. P. Chen, H. Chen, J. Qiu and C. Zhou, *Nano Res.*, **3**, 594 (2010).
3. M. Hilder, B. Winther-Jensen and N.B. Clark, *J. Power Sources*, **194,** 1135 (2009).
4. S. Lim, B. Kang, D. Kwak, W.H. Lee, J.A. Lim and K. Cho, *J. Phys. Chem. C*, **116**, 7520 (2012).
5. A.J. Bandodkar, V.W.S. Hung, W. Jia, G. Valdes-Ramirez, J.R. Windmiller, A.G. Martinez, J. Ramirez, G. Chan, K. Kerman and J. Wang, *Analyst*, **138**, 123 (2013).
6. J.T. Muth, D.M. Vogt, R.L. Truby, Y. Mengüç, D.B. Kolesky, R.J. Wood and J.A. Lewis, *Adv. Mater.*, **26**, 6307 (2014).
7. W. Jia, A.J. Bandodkar, G. Valdés-Ramírez, J.R. Windmiller, Z. Yang, J. Ramírez, G. Chan and J. Wang, *Anal. Chem.*, **85**, 6553 (2013).
8. Y. Lu, *Appl. Surf. Sci.*, **256**, 3554 (2010).
9. F.-Y. Shen, S.-E. Huang and W.-P. Dow, ECS Electrochem. Lett., **2**, D45 (2013).
10. Y. Kong, H. Chen, Y. Wang and S.A. Soper, *Electrophoresis*, **27**, 2940 (2006).
11. M.S. Miller, H.L. Filiatrault, G.J.E. Davidson, M. Luo and T.B. Carmichael, *J. Am. Chem. Soc.*, **132**, 762 (2009).
12. D. Zabetakis and W.J. Dressick, *ACS Appl. Mater. Interfaces*, **1**, 4 (2009).
13. R.O.F. Verkuijlen, M.H.A. van Dongen, A.A.E. Stevens, J. van Geldrop and J.P.C. Bernards, *Appl. Surf. Sci.*, **290**, 381 (2014).
14. S.H. Kim, S.W. Na, N.E. Lee, Y.W. Nam and Y.-H. Kim, *Surf. Coat. Tech.*, **200**, 2072 (2005).
15. M.S. Miller, G.J.E. Davidson, B.J. Sahli, C.M. Mailloux and T.B. Carmichael, *Adv. Mater.*, **20**, 59 (2008).
16. R.H. Guo, S.X. Jiang, Y.D. Zheng and J.W. Lan, *J. Appl. Polym. Sci.*, **127**, 4186 (2013).
17. Y.-C. Liao and Z.-K. Kao, *ACS App Mat Interf*, **4**, 5109 (2012).
18. D.I. Petukhov, M.N. Kirikova, A.A. Bessonov and M.J.A. Bailey, *Mater. Lett.*, **132**, 302 (2014).
19. T. Kazuhiko, O. Miki, K. Keisuke, C. Katsumi and U. Hirobumi, *Jpn. J. Appl. Phys.*, **53**, 05H (2014).
20. S. Onclin, B.J. Ravoo and D.N. Reinhoudt, *Angew. Chem. Int. Edit.*, **44**, 6282 (2005).
21. Y. Li, D. Chen, Q. Lu, X. Qian, Z. Zhu and J. Yin, *Appl. Surf. Sci.*, **241**, 471 (2005).
22. S. Sawada, Y. Masuda, P. Zhu and K. Koumoto, *Langmuir*, **22**, 332 (2005).
23. Guo, L. and DeWeerth, S. P., *Small*, **6**, 2847 (2010).
24. G. Corbelli, C. Ghisleri, M. Marelli, P. Milani, and L. Ravagnan, *Adv. Mater.*, **23**, 4504 (2011).
25. M. Zhu, M.Z. Lerum and W. Chen, *Langmuir*, **28**, 416 (2011).

Figures

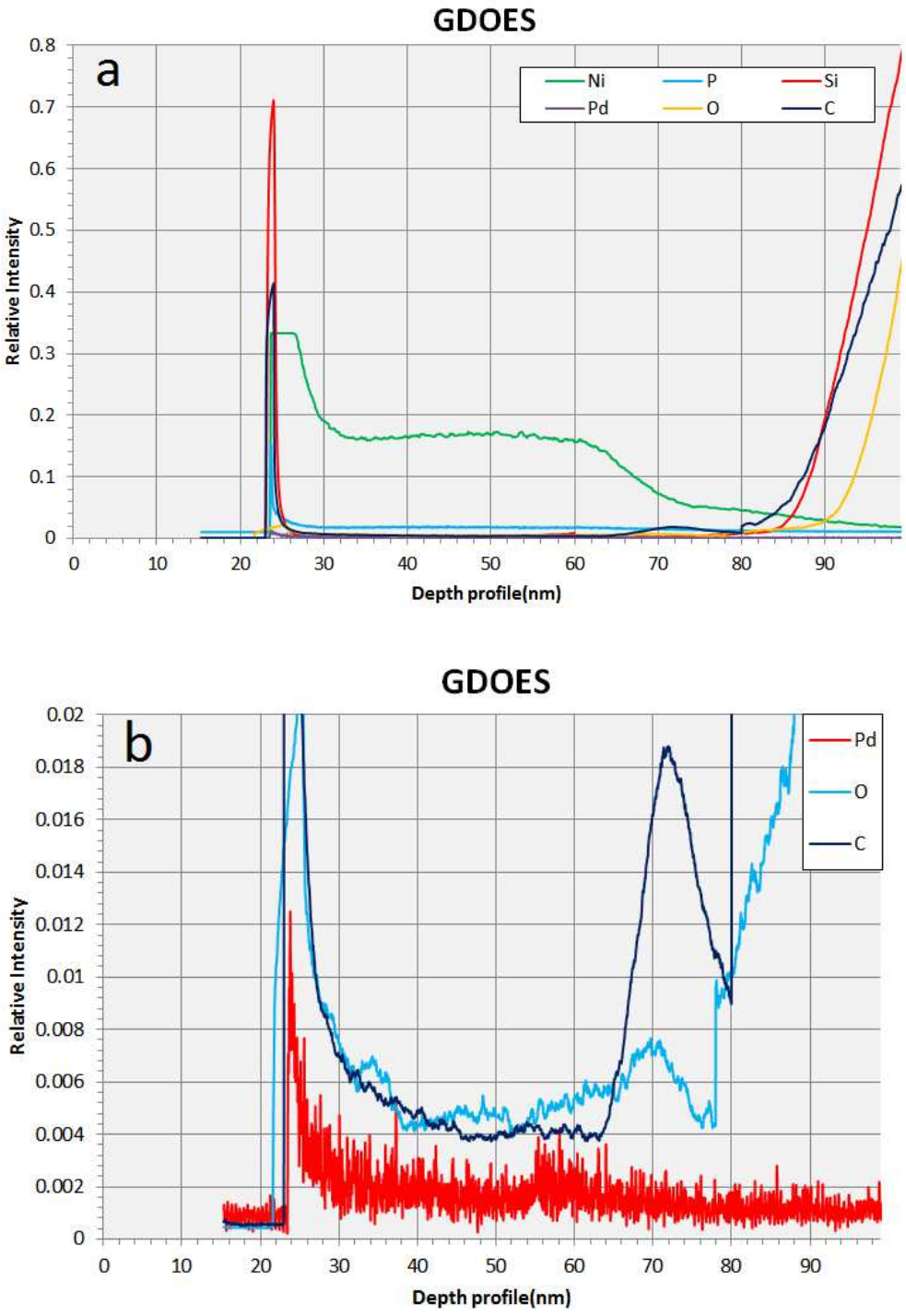

Figure 1. GDOES characterization of NiPB/PDMS (30s immersion in electroless solution) a) including all the signals and b) low intensity signals at PDMS/NiPB interface.

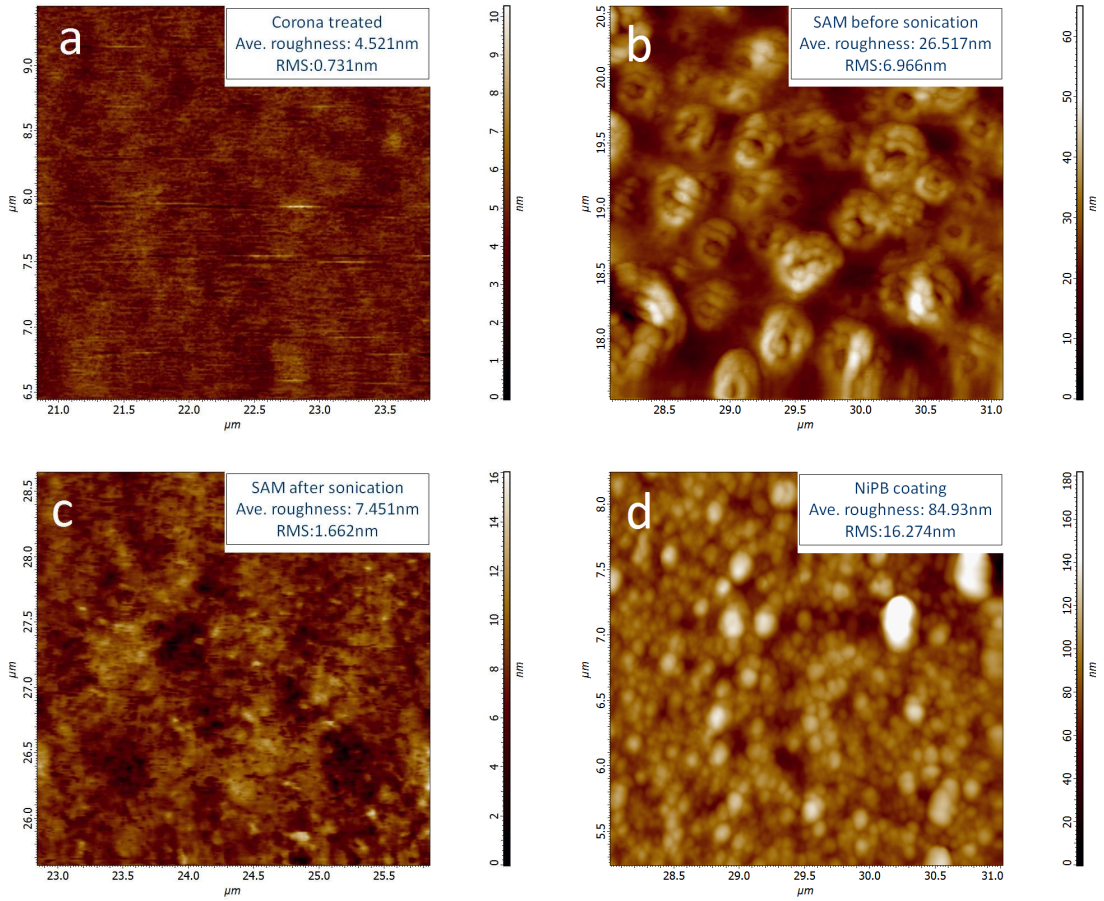

Figure 2. AFM characterization: a) corona treated surface, b) AEAPTMS treated surface, c) Silanized surface after 2 min toluene + 12 min DI water sonications and d) NiPB coating (30s immersion in electroless solution).

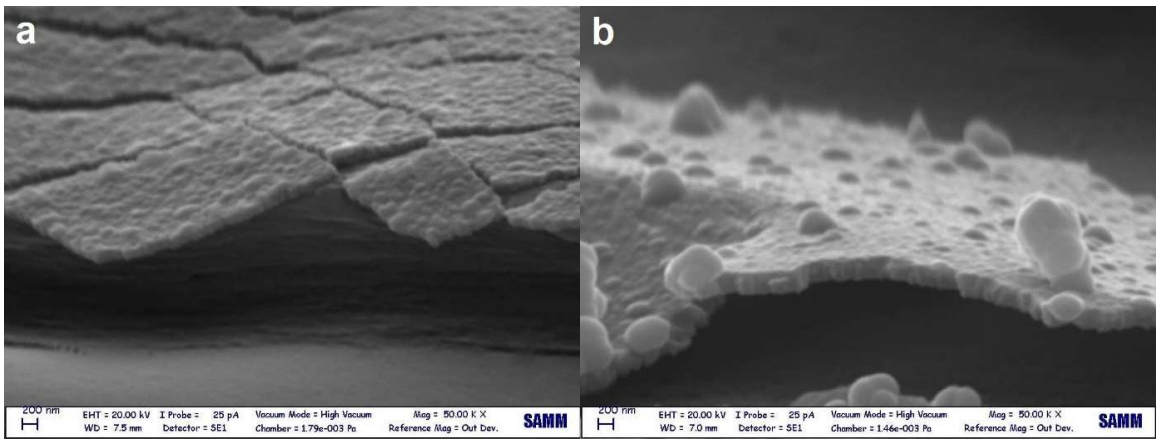

Figure 3. Cross-sectional SEM characterization of NiPB on PDMS (30s immersion in electroless solution): a) uniform morphology and b) nodular structure formation.

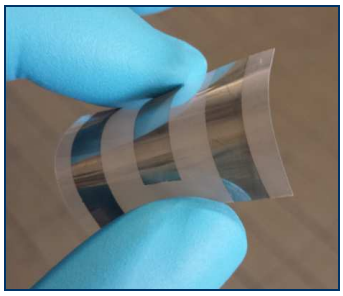

Figure 4. Three lines of NiPB coating (each line 5×20mm^2) on PDMS to employ as working, counter and reference electrodes for electrochemical studies.

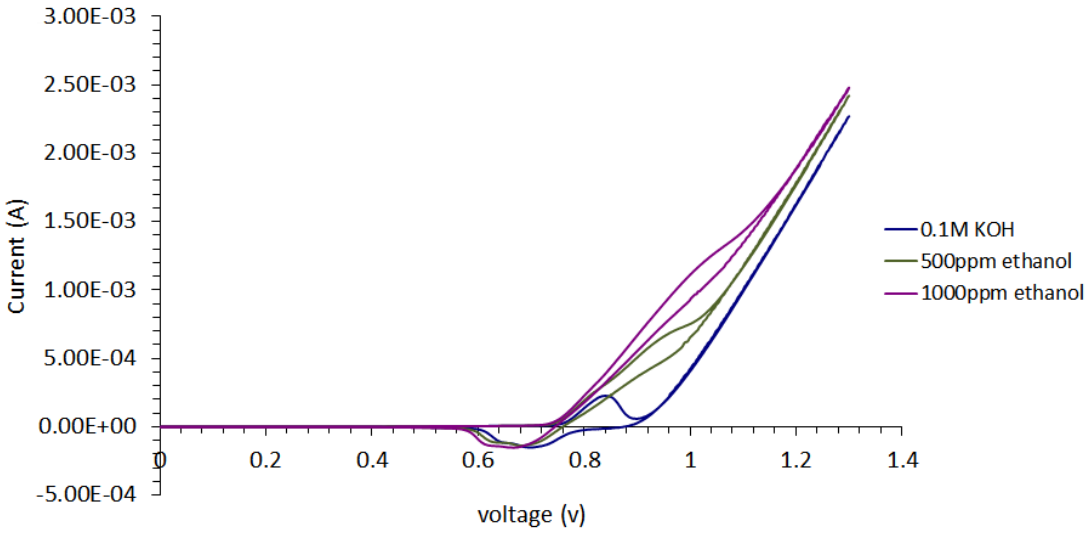

Figure 5. cyclic voltammograms of ethanol sensor: oxidation and reduction peaks corresponds to NiOOH/Ni(OH)$_2$ redox pair formation were detected between 0.6 to 0.9 V for 0.1M KOH. Oxidation of ethanol occurred around 0.9 V for 500ppm of ethanol.

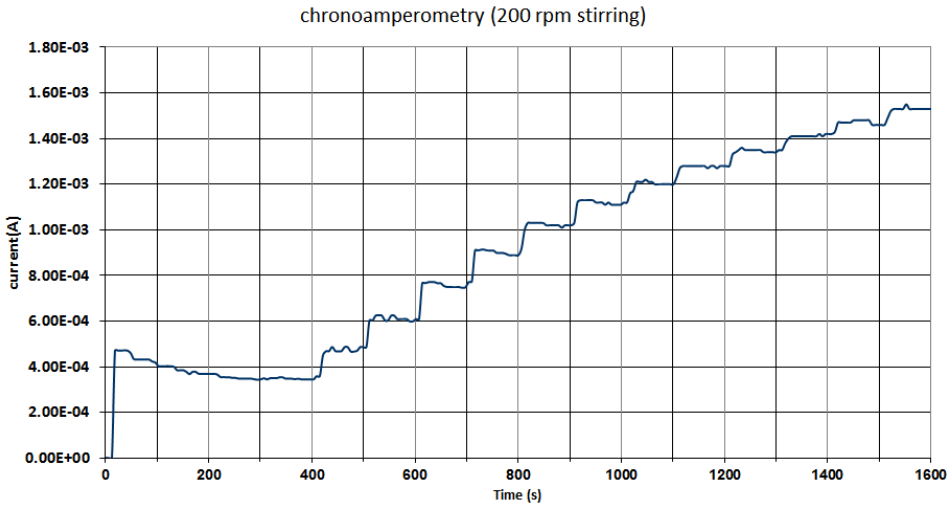

Figure 6. Amperometric response of ethanol sensor in 0.1M KOH solution during consecutive addition of ethanol every 100s. (Each step corresponds to 100ppm ethanol).

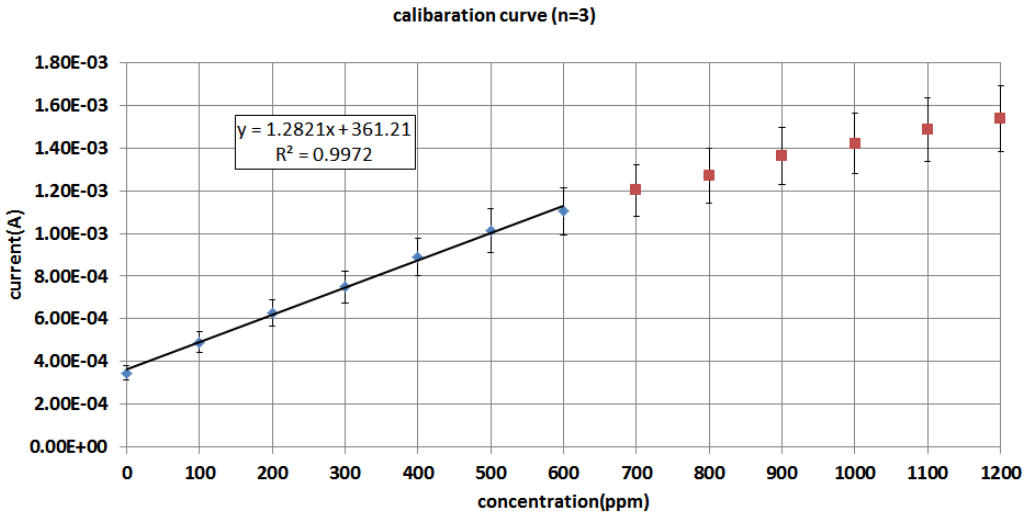

Figure 7. Calibration curve for ethanol sensor. The sensor sensitivity in the linear range is calculated as 6.9μA.ppm^{-1}.cm^{-2}.

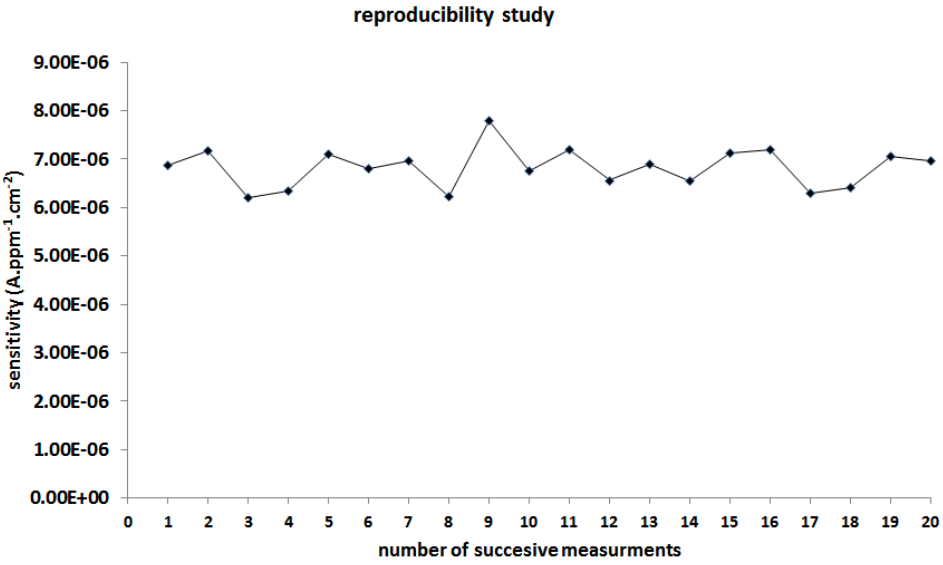

Figure 8. Sensor reproducibility studies: 20 times addition of 300ppm ethanol and their corresponding sensitivities. (Less than 10% variations)

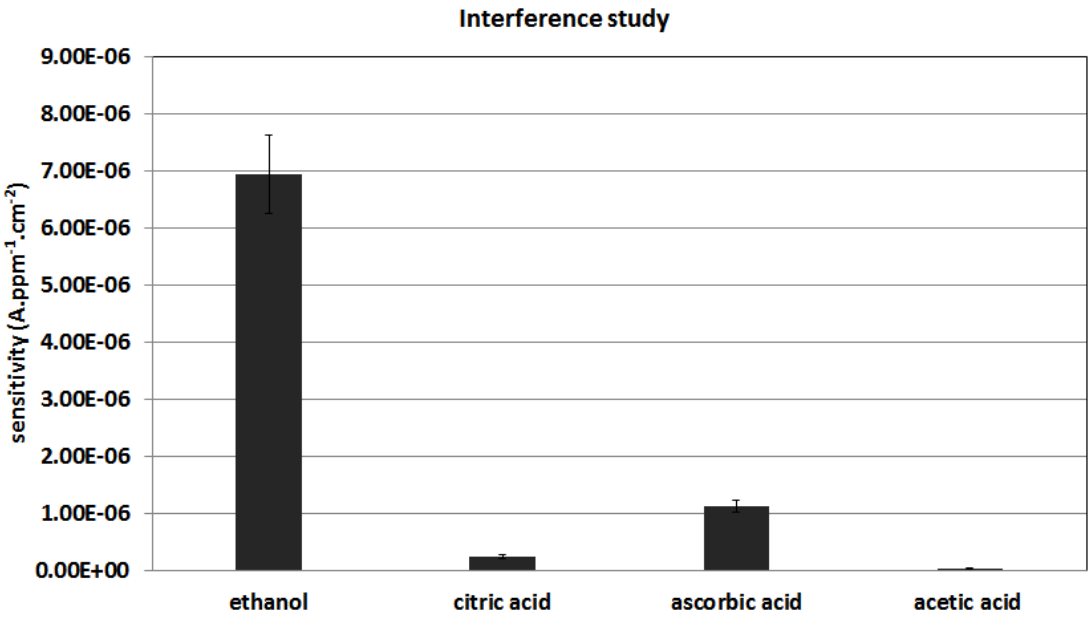

Figure 9. Interference studies of ethanol sensor in presence of citric acid, ascorbic acid and acetic acid.

Tables

Table I. NiPB Electroless Deposition Bath Provided by Tecnochimica (3000 Extra).

Source of Ni ion	Nickel Acetate
Reducing agents	$NaBH_4/NaH_2PO_2.xH_2O$ (1:100 w/w)
Complexing agent	Glycolic Acid
Ni ion concentration	6 g/l
P ion concentration	11 wt.%
Temperature	80 °C
pH	4.95
Deposition rate	10 µm/h